Supplementary Information (SI) for Journal of Materials Chemistry A.

Supporting Information

for

# Orchestrating Explainable AI, ChatGPT, and Human Expertise: A Framework for Extracting Polymer Design Guidelines

*Yin Kan Phua, Nana Terasoba, Manabu Tanaka, Tsuyohiko Fujigaya, Koichiro Kato*

**Building artificial neural network (ANN) models**

The entire workflow/process to build artificial neural network (ANN) models (Models I, II) are written in details below. The steps were the same for Model I and II, except for the number of hidden layers used. Model II-mini was built based on Model II, trained upon a dimensionally reduced database obtained after feature selection using Model II.

Data pre-processing:

1. Original dataset containing 346 types of anion exchange membrane (AEM) polymers with chemical structures converted to 3,226 descriptors were preprocessed by removing columns with nonnumerical values and empty rows.
2. Standard scaler was applied to database obtained from 1. Standard scaler standardizes the value of explanatory variables present in the database via subtracting the mean, followed by scaling to unit variance (dividing all values by standard deviation).

Statistical feature selection:

3. Variance threshold (threshold = 0) was applied to the database obtained from 2. Variance threshold eliminates explanatory variables with low variance, which are typically constant or nearly constant throughout the whole database. Such variables provide minute information during prediction and might be taken as noise by the model, hence removing these low-variance features typically lead to improvement in model performance.
4. Maximum relevance — minimum redundancy (mRMR) was applied to the database from 3. MRMR was set to reduce the number of explanatory variables to 1,000 dimensions, while keeping "Block A (*x*)", "Block B (1-*x*)", "Block A/B ratio", "Crosslinking [Yes/No]", "alkaline stability temperature [°C]", "Concentration of alkaline solution soaked in [mol/dm$^3$]", "alkaline stability [Days]", "Conductivity Measuring Temperature [°C]", and "IEC" if not included in the database after mRMR. mRMR is a statistical-based feature selection method that identifies features with the highest relevance to the target variable while minimizing redundancy among selected features. It achieves this by maximizing mutual information between each feature and the target, and simultaneously minimizing mutual information among the features themselves, resulting in a compact and informative subset that preserves essential data characteristics.[1, 2] The same pre-processing steps 3. and 4. were applied to test database, a database containing AEM polymers not included in the train database (termed unseen AEM polymers), as well.

Construction of ANN And Explainable machine learning (ML)-Based Feature Selection:

5. The database from 4. was used to train two ANN models (Model I and II). The hyperparameters tuned using Optuna for both models include: the number of neurons for each hidden layer (ranging from 2 to 600), the activation function (Rectified Linear Unit (ReLU), tanh, or logistic), the solver (stochastic gradient descent (SGD) or Adam), the initial learning rate (0.00001–0.01 on a logarithmic scale), the regularization parameter α (0.1–5 on a logarithmic scale), and the batch size (64, 128, 256, 512 or 1024) were automatically optimized by trial suggestions. The optimized hyperparameters for each model are as follows:

a. Model I used three hidden layers (Scheme S1a). The optimized hyperparameters are:

**Table S1**. Best hyperparameter settings of Model I.

| Hyperparameter | Best Settings |
|---|---|
| **Hidden Layer Sizes** | 512, 236, 64 |
| **Activation Function** | tanh |
| **Solver** | adam |
| **Initial Learning Rate** | 0.0001717234109928365 |
| **Regularization Parameter** | 4.446057291544881 |
| **Batch Size** | 1024 |

b. Model II used five hidden layers (Scheme S1b). The optimized hyperparameters are:

**Table S2**. Best hyperparameter settings of Model II.

| Hyperparameter | Best Settings |
|---|---|
| **Hidden Layer Sizes** | 502, 372, 144, 66, 34 |
| **Activation Function** | tanh |
| **Solver** | adam |
| **Initial Learning Rate** | 0.0009447269296114181 |
| **Regularization Parameter** | 0.27577818216283784 |
| **Batch Size** | 512 |

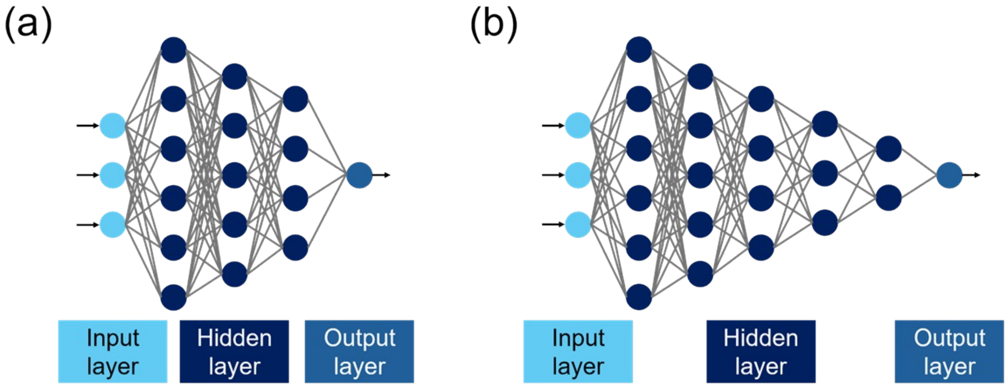

**Scheme S1**. ANN with (a) 3 hidden layers (Model I), and (b) with 5 hidden layers (Model II and II-mini).

6. Predictive performance of Model I and II were evaluated, with their train-validation prediction accuracy shown in Figure S1, and the model to be used for the remaining of this study was chosen based on their predictive performance towards test AEM polymers. Model II was found to be superior to Model I, with root mean square error (RMSE) for test prediction of 0.0230 S cm$^{-1}$ and 0.0349 S cm$^{-1}$, respectively. As such, Model II was used for explainable ML-based feature selection by applying ELI5 to Model II and selecting top 64 important explanatory variables.

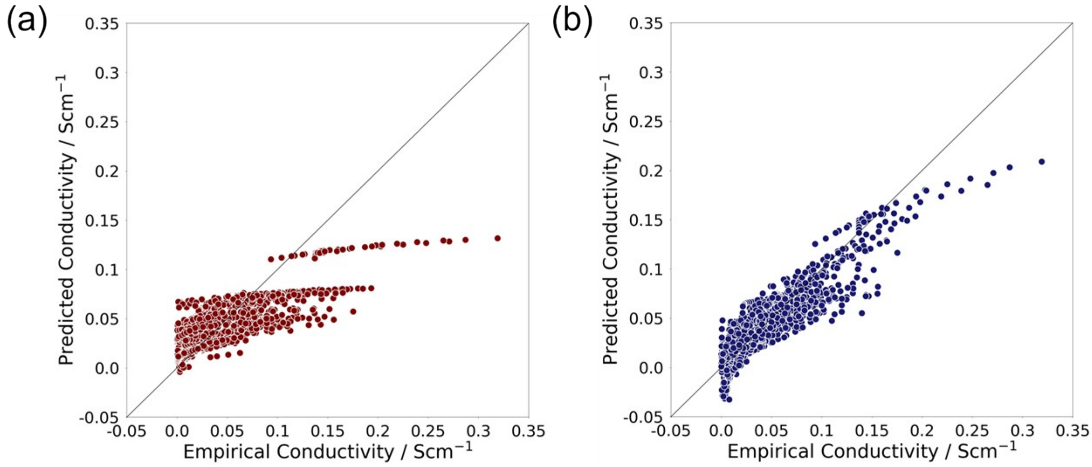

Figure S1. Predicted vs. actual anion conductivity plots from train-validation process of Models (a) I and (b) II.

## ELI5 Global Explanation Explanatory Variable Importance

ELI5 provides a built-in Permutation Importance class that estimates each feature's significance by measuring the overall deterioration in predictive performance when that feature is shuffled across all samples in the validation set. For a trained model $f$ and feature $j$:

1. Baseline Performance: Compute a baseline error metric $E$ (e.g., mean squared error, accuracy) on the validation set $D$.
2. Feature Shuffling: Permute feature $j$ across all samples in $D$, thereby destroying its original correlations.
3. Recompute Performance: Measure the new error $E'_j$ under this shuffled condition.
4. Importance Scoring: Define global permutation importance of feature $j$ as $\Delta j = E'_j - E$, indicating how much the model's performance degrades when feature $j$ is no longer informative.

Since the shuffling is performed at the dataset level, a single score $\Delta j$ per feature is obtained, reflecting that feature's overall contribution to predictive performance. This procedure is repeated for each feature $j$, yielding a global ranking.

**Table S3**. Top 64 important explanatory variables obtained through applying ELI5 to Model II, listed in descending order according to their importance.

| **Explanatory Variable Names** | **Weight** | **Standard Deviation** |
|---|---|---|
| **Conductivity Measuring Temperature / °C** | 0.300825 | 0.004159 |
| **Ion Exchange Capacity (IEC)** | 0.099787 | 0.002317 |
| **MATS1i_B** | 0.020753 | 0.001089 |
| **MATS5d_B** | 0.018965 | 0.001024 |
| **alkaline stability / Days** | 0.018214 | 0.000721 |
| **MATS2s_B** | 0.01419 | 0.000832 |
| **AATS8Z_A** | 0.013021 | 0.000699 |
| **AATSC5d_B** | 0.012452 | 0.00094 |

| | | |
|---|---|---|
| **MATS6c_A** | 0.010221 | 0.000725 |
| **AATS8v_A** | 0.009684 | 0.000208 |
| **VE3_DzZ_A** | 0.008531 | 0.001072 |
| **Block B (1-x)** | 0.008461 | 0.000515 |
| **AATS6d_A** | 0.008395 | 0.000902 |
| **Xc-5d_B** | 0.008303 | 0.000864 |
| **SpMax_A_A** | 0.008215 | 0.000911 |
| **AATSC1i_A** | 0.007873 | 0.001232 |
| **MATS4s_A** | 0.007784 | 0.000862 |
| **AATS7Z_A** | 0.00773 | 0.000948 |
| **AATS6p_A** | 0.007603 | 0.001123 |
| **TMWC10_B** | 0.007569 | 0.000927 |
| **GATS3se_A** | 0.007379 | 0.000373 |
| **MATS1i_A** | 0.007346 | 0.001328 |
| **ATSC5d_B** | 0.007268 | 0.00109 |
| **SpMAD_Dzm_B** | 0.007236 | 0.000366 |
| **AATS8se_A** | 0.007195 | 0.000782 |
| **ATSC6d_A** | 0.007067 | 0.000738 |
| **AATSC6c_A** | 0.007024 | 0.000198 |
| **AATSC2m_A** | 0.00698 | 0.000975 |
| **MATS1p_B** | 0.006968 | 0.00063 |
| **GATS3c_A** | 0.006823 | 0.000786 |
| **AATSC1i_B** | 0.006644 | 0.000236 |
| **MATS4se_B** | 0.006535 | 0.000244 |
| **MATS5i_A** | 0.006523 | 0.000624 |
| **MATS6s_A** | 0.006463 | 0.000855 |
| **AATS8are_A** | 0.006417 | 0.000358 |
| **MIC5_A** | 0.006338 | 0.000758 |
| **MATS4Z_B** | 0.005941 | 0.000719 |
| **MATS1c_A** | 0.00589 | 0.000372 |
| **Concentration of alkaline solution soaked in / mol dm$^{-3}$** | 0.005599 | 0.000951 |
| **ATSC0s_B** | 0.005539 | 0.000567 |
| **GATS6p_A** | 0.005505 | 0.00042 |
| **Xpc-4dv_A** | 0.005505 | 0.001369 |
| **BalabanJ_A** | 0.005452 | 0.000881 |
| **AATS8d_A** | 0.005327 | 0.000549 |

| | | |
|---|---|---|
| **AATSC5i_A** | 0.005321 | 0.000206 |
| **ATS3dv_A** | 0.005271 | 0.000468 |
| **GATS8s_A** | 0.005122 | 0.0004 |
| **AETA_eta_B_B** | 0.005017 | 0.000306 |
| **AATS3v_A** | 0.004992 | 0.001105 |
| **VSA_EState8_A** | 0.00497 | 0.000321 |
| **MATS5v_A** | 0.004944 | 0.000486 |
| **Block A (x)** | 0.004914 | 0.000314 |
| **AATSC2Z_A** | 0.004846 | 0.000207 |
| **AETA_eta_BR_B** | 0.004815 | 0.000585 |
| **MATS4pe_B** | 0.004802 | 0.000336 |
| **GATS8pe_A** | 0.00478 | 0.00043 |
| **bpol_A** | 0.004627 | 0.000922 |
| **SpAD_A_A** | 0.004499 | 0.000731 |
| **AATSC0m_A** | 0.004496 | 0.000724 |
| **SRW06_A** | 0.004485 | 0.000465 |
| **ATS4v_A** | 0.00448 | 0.000689 |
| **SpMAD_DzZ_B** | 0.004401 | 0.000877 |
| **GATS8are_A** | 0.004399 | 0.000411 |
| **SM1_Dzare_A** | 0.004377 | 0.000608 |

**Table S4.** Top 20 important explanatory variables obtained through applying ELI5 to Model II, and their explanations.

| Explanatory Variable Name | Type | Property Used | Lag | Chemical Meaning |
|---|---|---|---|---|
| **Conductivity Measuring Temperature / °C** | Experimental condition | — | — | Measuring temperature of anion conductivity. |
| **IEC** | Polymer characteristic | — | — | Ion exchange capacity of a polymer. |
| **MATS1i_B** | Moran autocorrelation; block B | Ionization potential | 1 | Measures how similarly ionization potential is distributed among directly bonded atoms in block B. |
| **MATS5d_B** | Moran autocorrelation; block B | Sigma electrons | 5 | Evaluates how sigma electron density is related across atoms five bonds apart in block B. |
| **alkaline stability / Days** | Experimental condition | — | — | Duration of alkaline stability test. |

| | | | | |
|---|---|---|---|---|
| **MATS2s_B** | Moran autocorrelation; block B | Intrinsic state | 2 | Captures how electronic configuration characteristics vary between atoms two bonds apart in block B. |
| **AATS8Z_A** | Averaged Moreau–Broto autocorrelation; block A | Atomic number | 8 | Assesses how atomic number varies across atom pairs eight bonds apart in block A. |
| **AATSC5d_B** | Centered avg. Moreau–Broto autocorrelation; block B | Sigma electrons | 5 | Evaluates variation in sigma electron density among atoms five bonds apart in block B, centered to mean. |
| **MATS6c_A** | Moran autocorrelation; block A | Gasteiger charge | 6 | Measures similarity in partial charges across atoms six bonds apart in block A. |
| **AATS8v_A** | Averaged Autocorrelation; block A | van der Waals volume | 8 | Atomic size spread over long range |
| **VE3_DzZ_A** | Eigenvector-based descriptor (Barysz matrix); block A | Atomic number | Eigenvector 3 | Captures global shape and branching of the molecule using atomic number and 3rd eigenvector components. |
| **Block B (1-x)** | Polymer characteristics | — | — | Molar ratio of block B. |
| **AATS6d_A** | Averaged Moreau–Broto autocorrelation; block A | Sigma electrons | 6 | Assesses how sigma electron count varies over 6-bond atom pairs in block A. |
| **Xc-5d_B** | Chi cluster index; block B | Sigma electrons | Order 5 | Reflects the local branching and electron density pattern in 5-atom clusters in block B. |
| **SpMax_A_A** | Spectral descriptor; block A | — | N/A | Indicates overall molecular branching through the largest eigenvalue of the adjacency matrix in block A. |
| **AATSC1i_A** | Centered avg. Moreau–Broto autocorrelation; block A | Ionization potential | 1 | Measures variation in ionization potential between bonded atoms in block A, normalized to mean. |
| **MATS4s_A** | Moran autocorrelation; block A | Intrinsic state | 4 | Describes how electronic configuration changes between atoms four bonds apart in block A. |
| **AATS7Z_A** | Averaged Moreau–Broto autocorrelation; block A | Atomic number | 7 | Shows how atomic number differences spread across 7-bond-separated atoms in block A. |
| **AATS6p_A** | Averaged Moreau–Broto autocorrelation; | Polarizability | 6 | Indicates how atomic polarizability varies across atoms six bonds apart in block |

|  |  |  |  |  |
|---|---|---|---|---|
|  | block A |  |  | A. |
| **TMWC10_B** | Total walk count; block B | — | Walk length = 10 | Quantifies the extent of atomic connectivity via the number of 10-step atom-atom paths in block B. |

**Model Prediction Logic Evaluation Using SHAP**

After using ELI5 to select the top 64 (actual = 67) important variables, the obtained train database was used to train Model II-mini. The hyperparameters tuned using Optuna for Model II-mini include: the number of neurons for each hidden layer (ranging from 2 to 48), the activation function (Rectified Linear Unit (ReLU), tanh, or logistic), the solver (stochastic gradient descent (SGD) or Adam), the initial learning rate (0.000005–0.01 on a logarithmic scale), the regularization parameter α (0.001–1.2 on a logarithmic scale), and the batch size (64, 128, 256, 512 or 1024) were automatically optimized by trial suggestions. The optimized hyperparameters for each model are as follows:

**Table S5**. Best hyperparameter settings of Model II-mini.

| Hyperparameter | Best Settings |
|---|---|
| **Hidden Layer Sizes** | 34, 22, 16, 8, 2 |
| **Activation Function** | tanh |
| **Solver** | adam |
| **Initial Learning Rate** | 0.0019061299275277247 |
| **Regularization Parameter** | 0.005890339596103016 |
| **Batch Size** | 64 |

SHAP was applied to Model II-mini, but not to Model II directly because calculating SHAP value for each variable requires huge amount of computation resources (Fig. S2a).

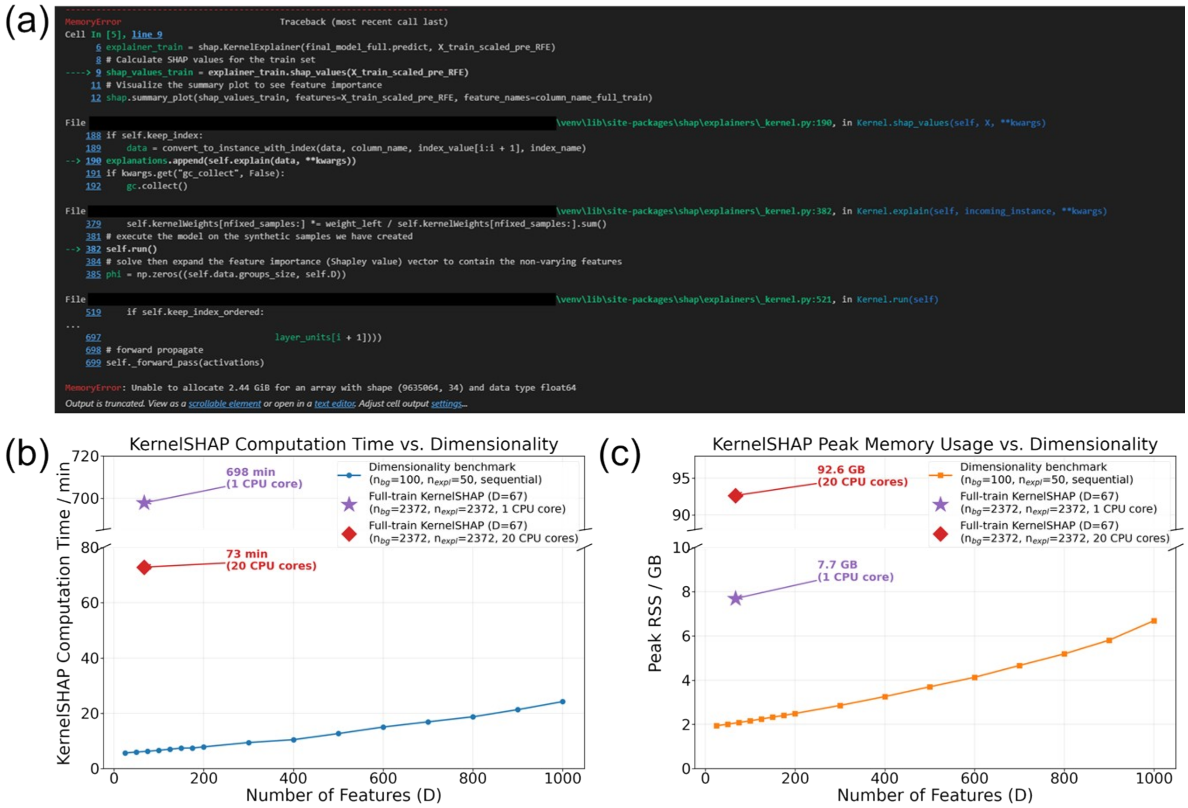

```
MemoryError                               Traceback (most recent call last)
Cell In [5], line 9
      6 explainer_train = shap.KernelExplainer(final_model_full.predict, X_train_scaled_pre_RFE)
      8 # Calculate SHAP values for the train set
----> 9 shap_values_train = explainer_train.shap_values(X_train_scaled_pre_RFE)
     11 # Visualize the summary plot to see feature importance
     12 shap.summary_plot(shap_values_train, features=X_train_scaled_pre_RFE, feature_names=column_name_full_train)

File [redacted]\venv\lib\site-packages\shap\explainers\_kernel.py:190, in Kernel.shap_values(self, X, **kwargs)
    188 if self.keep_index:
    189     data = convert_to_instance_with_index(data, column_name, index_value[i:i + 1], index_name)
--> 190 explanations.append(self.explain(data, **kwargs))
    191 if kwargs.get("gc_collect", False):
    192     gc.collect()

File [redacted]\venv\lib\site-packages\shap\explainers\_kernel.py:382, in Kernel.explain(self, incoming_instance, **kwargs)
    379     self.kernelWeights[nfixed_samples:] *= weight_left / self.kernelWeights[nfixed_samples:].sum()
    381 # execute the model on the synthetic samples we have created
--> 382 self.run()
    384 # solve then expand the feature importance (Shapley value) vector to contain the non-varying features
    385 phi = np.zeros((self.data.groups_size, self.D))

File [redacted]\venv\lib\site-packages\shap\explainers\_kernel.py:521, in Kernel.run(self)
    519     if self.keep_index_ordered:
...
    697                                         layer_units[i + 1])))
    698 # forward propagate
    699 self._forward_pass(activations)

MemoryError: Unable to allocate 2.44 GiB for an array with shape (9635064, 34) and data type float64
Output is truncated. View as a scrollable element or open in a text editor. Adjust cell output settings...
```

**Figure S2**. (a) Memory error message when trying to apply SHAP to Model II. Black boxes were placed over the portion of path directory to protect private information. The computation environment used was: Intel Core i9-11900K, 64 GB system memory, NVIDIA RTX 3060 graphics card. Python version: 3.9.7. KernelSHAP computational scaling with feature dimensionality. (b) Computation time and (c) peak memory usage (RSS) as a function of feature dimensionality D, benchmarked using an MLPregressor with the same hyperparameter settings as Model II, trained separately at each D using randomly selected descriptors ($n_{\text{background}}$ = 100, $n_{\text{explain}}$ = 50, $n_{\text{samples}} \approx 2D + 2048$). The dashed green line indicates D = 67 (Model II-mini, post-ELI5 feature selection). Both metrics increase monotonically with D, confirming that dimensionality reduction is essential for computationally feasible SHAP analysis of high-dimensional molecular descriptor datasets. The computational resource used for KernelSHAP computational scaling was: Intel Core i9-14900K, 192 GB (128 GB allocated for Windows Subsystem for Linux 2), NVIDIA RTX 4080 graphics card.

**Table S6**. KernelSHAP (KernelExplainer) computational benchmarks under controlled and manuscript-style settings. Runtime and peak RSS (Python process resident set size) were measured via subprocess monitoring of /proc/[pid]/status at 50 ms intervals. Per-thread Basic Linear Algebra Subprograms (BLAS) parallelism was limited (OMP_NUM_THREADS = MKL_NUM_THREADS = OPENBLAS_NUM_THREADS = 1) unless otherwise noted. Default KernelSHAP sampling was used ($n_{\text{samples}} \approx 2D + 2048$). Computational resource used: 192 GB (128 GB allocated for Windows Subsystem for Linux 2). (Panel A) Controlled scaling benchmark (fixed background and explained set). At each D, an MLP with the same hyperparameter settings as Model II was trained separately using randomly selected descriptors from the full feature set. $n_{\text{background}}$ = 100 (*k*-means cluster centers); $n_{\text{explain}}$ = 50; sequential (1 core). (Panel B) Manuscript-style feasibility benchmark (full training set). Model II-mini architecture (hidden layers: 34, 22, 16, 8, 2) was used with the entire training set as both background and explained data. Parallel configuration distributed evaluation across 20 CPU cores using joblib.

| **Benchmark Regime** | **Setting** | **D** | **$n_{samples}$** | **$n_{background}$** | **$n_{explain}$** | **Cores** | **Time / min** | **Peak RSS / GB** |
|---|---|---|---|---|---|---|---|---|
| **Panel A — Controlled scaling benchmark** | | | | | | | | |
| Controlled | Sequential | 25 | 2,098 | 100 | 50 | 1 | 5.67 | 1.94 |
| Controlled | Sequential | 50 | 2,148 | 100 | 50 | 1 | 5.98 | 2.01 |
| Controlled | Sequential | 100 | 2,248 | 100 | 50 | 1 | 6.63 | 2.16 |
| Controlled | Sequential | 200 | 2,448 | 100 | 50 | 1 | 7.86 | 2.49 |
| Controlled | Sequential | 400 | 2,848 | 100 | 50 | 1 | 10.46 | 3.26 |
| Controlled | Sequential | 600 | 3,248 | 100 | 50 | 1 | 15.04 | 4.13 |
| Controlled | Sequential | 800 | 3,648 | 100 | 50 | 1 | 18.74 | 5.19 |
| Controlled | Sequential | 1000 | 4,048 | 100 | 50 | 1 | 24.23 | 6.69 |
| **Panel B — Manuscript-style feasibility benchmark** | | | | | | | | |
| Manuscript-style | Sequential | 67 | 2,182 | 2,372 | 2,372 | 1 | 697.7 | 7.69 |
| Manuscript-style | Parallel | 67 | 2,182 | 2,372 | 2,372 | 20 | 72.9 | 92.64 |

Parallelization achieved a 9.6× speed-up at the cost of a 12.0× increase in peak memory, as each parallel process (one per CPU core) instantiates its own KernelExplainer with associated internal allocations.

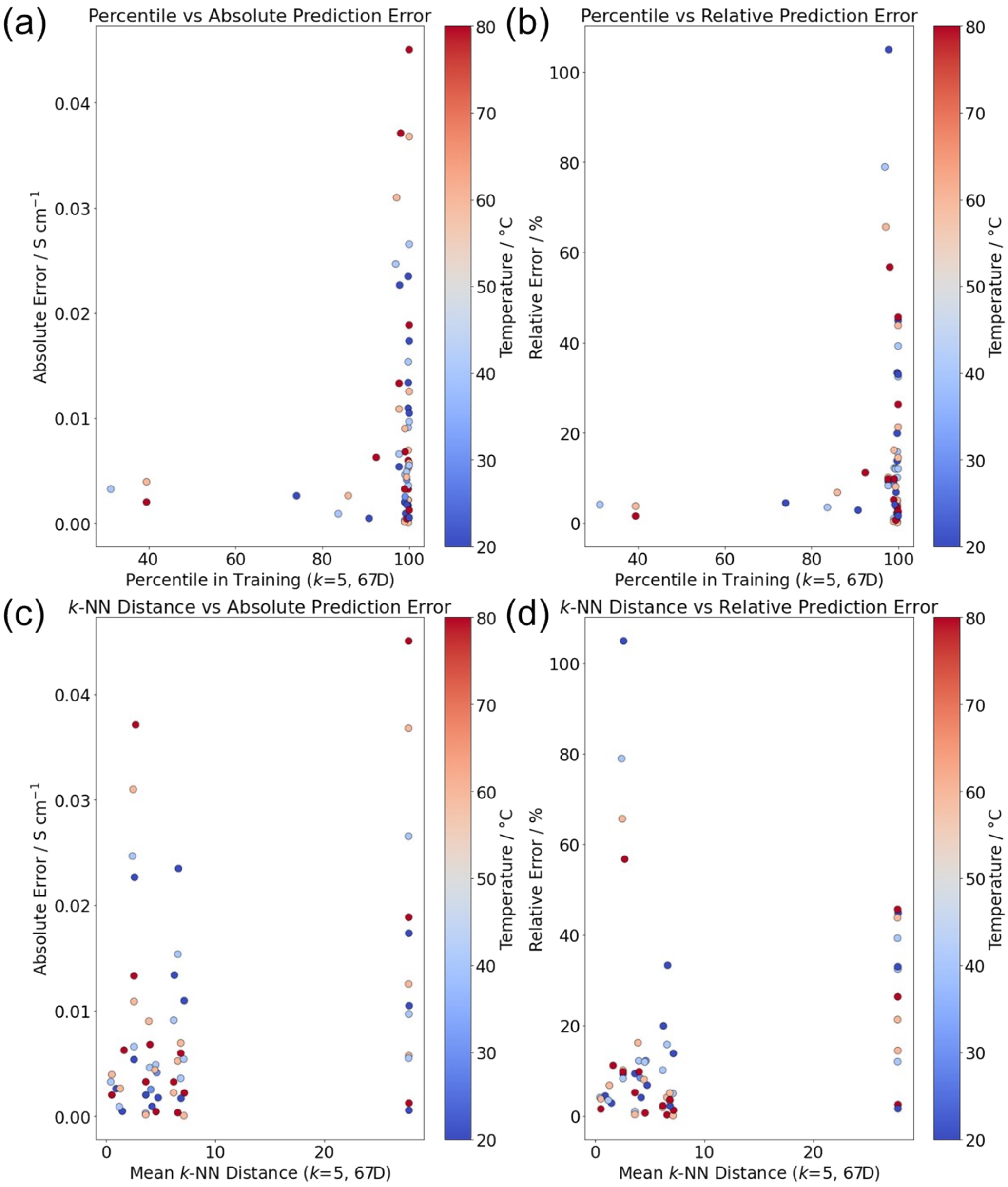

**Figure S3**. Relationship between applicability-domain metrics and prediction error for the 58 held-out test data points (14 polymers at multiple temperatures). (a) Percentile ranking (relative to training-set internal *k*-nearest neighbor (*k*-NN) distance distribution) vs. absolute prediction error. (b) Percentile ranking vs. relative prediction error. (c) Mean *k*-NN distance (standardized 67-dimensional descriptor space, $k$ = 5 (default), Euclidean) vs. absolute prediction error. (d) Mean *k*-NN distance vs. relative prediction error. Points are colored by measurement temperature (colorbar). The analysis reveals that most test points cluster in the 97–100% percentile range with widely varying errors, whereas *k*-NN distance provides better separation: data points with *k*-NN distances ≤7.2 generally exhibit low absolute errors (MAE ≤ 0.015 S cm$^{-1}$), while those with substantially larger distances (~27.7, PAEK-HQACz[3] group) show elevated errors. The 95th percentile of the training-dataset internal k-NN distance distribution serves as a conservative reference; however, 50 of 58 test points exceed this threshold while the model retains strong overall predictive accuracy (test set RMSE = 0.0136 S cm$^{-1}$, MAE = 0.0089 S cm$^{-1}$), indicating that absolute *k*-NN distance is a more informative predictor of reliability than percentile ranking alone. Qualitative conclusions are unchanged for $k$ = 2–10.

**Table S7**. Applicability-domain analysis for held-out test polymers and conceptual AEM Polymer designs evaluated with Model II-mini. *k*-NN distances (*k* = 5, Euclidean) were computed in the standardized 67-dimensional descriptor space, with percentile rankings relative to the training-set internal *k*-NN distance distribution. The table reports mean, minimum, and maximum *k*-NN distances across the *k* nearest neighbors, along with the percentile rank and whether each data point falls within the 95th percentile reference threshold. Test polymers (14 unique polymers, 58 data points at multiple temperatures) are from four independent studies; conceptual AEM Polymer designs 1–4 are evaluated at 80 °C. Test polymers with *k*-NN distances ≤ 7.2 generally exhibit strong predictive accuracy, whereas those with substantially larger distances (~27.7, PAEK-HQACz[3] group) show degraded predictions. The four conceptual designs exhibit *k*-NN distances of 4.71–6.90, placing them within the range of well-predicted test polymers. Qualitative conclusions are unchanged for *k* = 2–10.

| **DOI** | **Membrane Name** | **data set** | **Temperature / °C** | **Mean kNN distance** | **Min kNN distance** | **Max kNN distance** | **Percentile in train** | **Within 95pct** |
|---|---|---|---|---|---|---|---|---|
| 10.1039/D2TA03862E | PTPipQ100 | test | 20 | 0.935299 | 0.445259 | 1.55968 | 74.07251 | TRUE |
| 10.1039/D2TA03862E | PTPipQ100 | test | 40 | 0.445259 | 2.25E-14 | 0.890518 | 31.28162 | TRUE |
| 10.1039/D2TA03862E | PTPipQ100 | test | 60 | 0.534311 | 2.25E-14 | 0.890518 | 39.50253 | TRUE |
| 10.1039/D2TA03862E | PTPipQ100 | test | 80 | 0.534311 | 2.25E-14 | 1.335777 | 39.50253 | TRUE |
| 10.1039/D2TA03862E | PTPipQ83 | test | 20 | 2.571135 | 2.54561 | 2.588705 | 97.68128 | FALSE |
| 10.1039/D2TA03862E | PTPipQ83 | test | 40 | 2.570591 | 2.54561 | 2.588705 | 97.68128 | FALSE |
| 10.1039/D2TA03862E | PTPipQ83 | test | 60 | 2.570591 | 2.54561 | 2.588705 | 97.68128 | FALSE |
| 10.1039/D2TA03862E | PTPipQ83 | test | 80 | 2.570591 | 2.54561 | 2.588705 | 97.68128 | FALSE |
| 10.1039/D2TA03862E | PpTASU | test | 20 | 6.652945 | 6.569944 | 6.717292 | 99.78921 | FALSE |
| 10.1039/D2TA03862E | PpTASU | test | 40 | 6.593556 | 6.554839 | 6.658002 | 99.78921 | FALSE |
| 10.1039/D2TA03862E | PpTASU | test | 60 | 6.584967 | 6.554839 | 6.615053 | 99.78921 | FALSE |
| 10.1039/D2TA03862E | PpTASU | test | 80 | 6.593556 | 6.554839 | 6.658002 | 99.78921 | FALSE |
| 10.1039/D2TA03862E | PpTDMP | test | 20 | 7.174089 | 7.051777 | 7.244613 | 99.78921 | FALSE |
| 10.1039/D2TA03862E | PpTDMP | test | 40 | 7.131088 | 7.051777 | 7.215233 | 99.78921 | FALSE |
| 10.1039/D2TA03862E | PpTDMP | test | 60 | 7.146744 | 7.037706 | 7.215233 | 99.78921 | FALSE |
| 10.1039/D2TA03862E | PpTDMP | test | 80 | 7.187408 | 7.093823 | 7.230917 | 99.78921 | FALSE |
| 10.1039/D2TA03862E | PmTASU | test | 20 | 6.275044 | 6.187005 | 6.343254 | 99.78921 | FALSE |
| 10.1039/D2TA03862E | PmTASU | test | 40 | 6.212058 | 6.170962 | 6.280434 | 99.78921 | FALSE |
| 10.1039/D2TA03862E | PmTASU | test | 60 | 6.202949 | 6.170962 | 6.234885 | 99.78921 | FALSE |

| | | | | | | | | |
|---|---|---|---|---|---|---|---|---|
| 10.1039/D2TA03862E | PmTASU | test | 80 | 6.212058 | 6.170962 | 6.280434 | 99.78921 | FALSE |
| 10.1039/D2TA03862E | PmTDMP | test | 20 | 6.877332 | 6.8447 | 6.923903 | 99.78921 | FALSE |
| 10.1039/D2TA03862E | PmTDMP | test | 40 | 6.84993 | 6.830203 | 6.885345 | 99.78921 | FALSE |
| 10.1039/D2TA03862E | PmTDMP | test | 60 | 6.855709 | 6.830203 | 6.888011 | 99.78921 | FALSE |
| 10.1039/D2TA03862E | PmTDMP | test | 80 | 6.860538 | 6.830203 | 6.909571 | 99.78921 | FALSE |
| 10.1021/acs.iecr.1c04171 | PPO-Pip | test | 20 | 1.501055 | 0.313291 | 2.535559 | 90.76728 | TRUE |
| 10.1021/acs.iecr.1c04171 | PPO-Pip | test | 40 | 1.222339 | 0.313291 | 2.101985 | 83.68465 | TRUE |
| 10.1021/acs.iecr.1c04171 | PPO-Pip | test | 60 | 1.309054 | 0.313291 | 2.535559 | 85.96121 | TRUE |
| 10.1021/acs.iecr.1c04171 | PPO-Pip | test | 80 | 1.657729 | 0.313291 | 2.687393 | 92.41147 | TRUE |
| 10.1021/acs.iecr.1c04171 | PPO-OPip | test | 20 | 3.652812 | 3.557485 | 3.726523 | 98.94604 | FALSE |
| 10.1021/acs.iecr.1c04171 | PPO-OPip | test | 40 | 3.640957 | 3.557485 | 3.710622 | 98.94604 | FALSE |
| 10.1021/acs.iecr.1c04171 | PPO-OPip | test | 60 | 3.640957 | 3.557485 | 3.710622 | 98.94604 | FALSE |
| 10.1021/acs.iecr.1c04171 | PPO-OPip | test | 80 | 3.652812 | 3.557485 | 3.726523 | 98.94604 | FALSE |
| 10.1021/acs.iecr.1c04171 | PPO-PipOH | test | 20 | 2.61907 | 1.982621 | 3.253794 | 97.80776 | FALSE |
| 10.1021/acs.iecr.1c04171 | PPO-PipOH | test | 40 | 2.428706 | 1.982621 | 3.148925 | 96.92243 | FALSE |
| 10.1021/acs.iecr.1c04171 | PPO-PipOH | test | 60 | 2.492741 | 1.982621 | 3.469098 | 97.13322 | FALSE |
| 10.1021/acs.iecr.1c04171 | PPO-PipOH | test | 80 | 2.723426 | 1.982621 | 3.469098 | 98.06071 | FALSE |
| 10.1002/adfm.201902059 | F20C9N | test | 20 | 4.225305 | 3.76329 | 4.717406 | 99.19899 | FALSE |
| 10.1002/adfm.201902059 | F20C9N | test | 30 | 4.11201 | 3.78954 | 4.615144 | 99.07251 | FALSE |
| 10.1002/adfm.201902059 | F20C9N | test | 40 | 4.006738 | 3.76329 | 4.372499 | 99.03035 | FALSE |
| 10.1002/adfm.201902059 | F20C9N | test | 60 | 3.930904 | 3.76329 | 4.163465 | 99.03035 | FALSE |
| 10.1002/adfm.201902059 | F20C9N | test | 80 | 4.039732 | 3.76329 | 4.615144 | 99.07251 | FALSE |
| 10.1002/adfm.201902059 | H22C9N | test | 20 | 4.780602 | 4.345599 | 5.32397 | 99.4941 | FALSE |
| 10.1002/adfm.201902059 | H22C9N | test | 30 | 4.653355 | 4.368351 | 5.101121 | 99.45194 | FALSE |
| 10.1002/adfm.201902059 | H22C9N | test | 40 | 4.559302 | 4.345599 | 4.882686 | 99.40978 | FALSE |
| 10.1002/adfm.201902059 | H22C9N | test | 60 | 4.492018 | 4.345599 | 4.696416 | 99.40978 | FALSE |
| 10.1002/adfm.201902059 | H22C9N | test | 80 | 4.589478 | 4.345599 | 5.101121 | 99.45194 | FALSE |
| 10.1016/j.memsci.2021.119079 | PAEK-HQACz-0.5 | test | 20 | 27.78548 | 27.7498 | 27.8354 | 100 | FALSE |
| 10.1016/j.memsci.2021.11907 | PAEK-HQACz- | test | 40 | 27.75694 | 27.74623 | 27.77836 | 100 | FALSE |

| | | | | | | | | |
|---|---|---|---|---|---|---|---|---|
| 9 | 0.5 | | | | | | | |
| 10.1016/j.memsci.2021.119079 | PAEK-HQACz-0.5 | test | 60 | 27.75337 | 27.74623 | 27.76052 | 100 | FALSE |
| 10.1016/j.memsci.2021.119079 | PAEK-HQACz-0.5 | test | 80 | 27.76765 | 27.74623 | 27.80333 | 100 | FALSE |
| 10.1016/j.memsci.2021.119079 | PAEK-HQACz-0.6 | test | 20 | 27.76484 | 27.72913 | 27.81479 | 100 | FALSE |
| 10.1016/j.memsci.2021.119079 | PAEK-HQACz-0.6 | test | 40 | 27.73628 | 27.72555 | 27.75771 | 100 | FALSE |
| 10.1016/j.memsci.2021.119079 | PAEK-HQACz-0.6 | test | 60 | 27.7327 | 27.72555 | 27.73985 | 100 | FALSE |
| 10.1016/j.memsci.2021.119079 | PAEK-HQACz-0.6 | test | 80 | 27.74699 | 27.72555 | 27.7827 | 100 | FALSE |
| 10.1016/j.memsci.2021.119079 | PAEK-HQACz-0.7 | test | 20 | 27.75665 | 27.72093 | 27.80662 | 100 | FALSE |
| 10.1016/j.memsci.2021.119079 | PAEK-HQACz-0.7 | test | 40 | 27.72808 | 27.71735 | 27.74952 | 100 | FALSE |
| 10.1016/j.memsci.2021.119079 | PAEK-HQACz-0.7 | test | 60 | 27.7245 | 27.71735 | 27.73165 | 100 | FALSE |
| 10.1016/j.memsci.2021.119079 | PAEK-HQACz-0.7 | test | 80 | 27.73879 | 27.71735 | 27.77451 | 100 | FALSE |
| — | AEM Polymer 1 | conceptual | 80 | 6.792802 | 6.780324 | 6.80264 | 99.78921 | FALSE |
| — | AEM Polymer 2 | conceptual | 80 | 5.149477 | 5.060436 | 5.235003 | 99.70489 | FALSE |
| — | AEM Polymer 3 | conceptual | 80 | 4.711315 | 4.631919 | 4.777318 | 99.4941 | FALSE |
| — | AEM Polymer 4 | conceptual | 80 | 6.901414 | 6.84689 | 6.954268 | 99.78921 | FALSE |

**Table S8**. Top 20 important variables obtained from applying SHAP to Model II-mini, and their explanations.

| Explanatory Variable Name | Type | Property Used | Lag | Chemical Meaning |
|---|---|---|---|---|
| **AATSC5i_A** | Averaged & Centered Autocorrelation; block A | Ionization potential | 5 | Electron distribution across 5-bond distances |
| **AATS8v_A** | Averaged Autocorrelation; block A | van der Waals volume | 8 | Atomic size spread over long range |
| **Conductivity Measuring Temperature / °C** | Experimental condition | — | — | Measuring temperature of anion conductivity. |
| **SRW06_A** | Self-Returning Walk Count; block A | Topological structure | 6 | Cyclicity and local structural complexity |
| **AATSC2Z_A** | Centered averaged Moreau-Broto autocorrelation; block A | Atomic number | 2 | Measures similarity in atomic number between atoms two bonds apart, normalized by mean. |
| **TMWC10_B** | Total walk count; block B | — | Walk length = 10 | Reflects the extent of atomic connectivity via all possible paths of length 10. |
| **GATS6p_A** | Geary autocorrelation; block A | Polarizability | 6 | Evaluates how polarizability differs between atoms six bonds apart. |
| **GATS8are_A** | Geary autocorrelation; block A | Allred-Rochow electronegativity | 8 | Assesses difference in Allred-Rochow EN between distant atoms (8-bond distance). |
| **AATSC5d_B** | Centered averaged Moreau-Broto autocorrelation; block B | Sigma electrons | 5 | Describes variation in sigma electron count across atoms five bonds apart in block B. |

| | | | | |
|---|---|---|---|---|
| **ATS3dv_A** | Moreau-Broto autocorrelation; block A | Valence electrons | 3 | Shows how valence electron counts are distributed between atoms three bonds apart. |
| **AATSC2m_A** | Centered averaged Moreau-Broto autocorrelation; block A | Mass | 2 | Describes mass similarity between atoms separated by two bonds. |
| **IEC** | Polymer characteristic | — | — | Ion exchange capacity of a polymer. |
| **AATS7Z_A** | Averaged Moreau-Broto autocorrelation; block A | Atomic number | 7 | Evaluates variation in atomic number across atoms seven bonds apart. |
| **GATS3se_A** | Geary autocorrelation; block A | Sanderson electronegativity | 3 | Measures difference in Sanderson EN between atoms three bonds apart. |
| **SpMAD_DzZ_B** | Spectral mean absolute deviation; block B | Atomic number | — | Captures variability of atomic number contributions from the Barysz matrix in block B. |
| **MATS4se_B** | Moran autocorrelation; block B | Sanderson electronegativity | 4 | Measures similarity in Sanderson EN between atoms four bonds apart in block B. |
| **MATS5i_A** | Moran autocorrelation; block A | Ionization potential | 5 | Describes how ionization potential correlates between atoms five bonds apart in block A. |
| **GATS3c_A** | Geary autocorrelation; block A | Gasteiger charge | 3 | Evaluates charge differences (Gasteiger) among atoms three bonds apart. |
| **AETA_eta_BR_B** | ETA branching index; block B | — | Ring count | Quantifies molecular branching in block B considering the number |

| | | | | |
|---|---|---|---|---|
| | | | | of rings. |
| **GATS8pe_A** | Geary autocorrelation; block A | Pauling electronegativity | 8 | Quantifies long-range electronegativity dissimilarity at 8-bond separation (Geary Coefficient). |

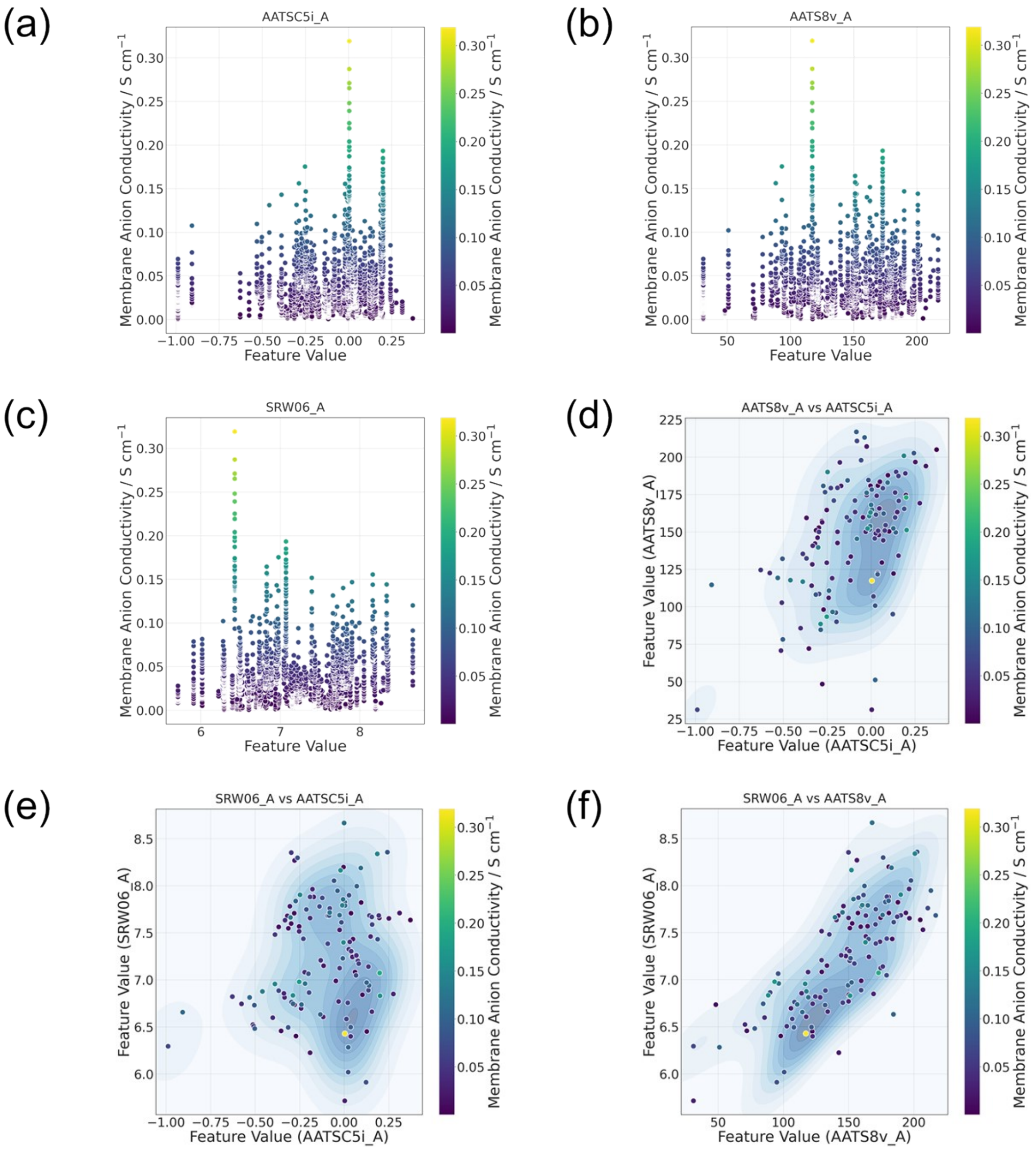

**Figure S4**. Scatter plot of descriptor value vs. anion conductivity for (a) AATSC5i_A, (b) AATS8v_A, and (c) SRW06_A. Scatter plot of descriptor value vs. descriptor value for the descriptor pairs (d) AATS8v_A vs. AATSC5i_A, (e) SRW06_A vs. AATSC5i_A, (f) SRW06_A vs. AATS8v_A. The color corresponds to anion conductivity value, with higher value shown in bright yellow, and lower value in dark purple. Blue color background represents density plot calculated according to datapoint count and their magnitude of anion conductivity, where darker blue represents higher density of datapoints with higher anion conductivity.

**Table S9**. Representative examples of ChatGPT output refinement through human-in-the-loop validation. ChatGPT served as an interpretive accelerator to generate initial draft explanations from source code and formal definitions; expert validation ensured scientific accuracy, appropriate epistemic humility, and practical relevance before incorporation into design guidelines.

| Task | Typical LLM Tendency Observed | Expert Correction/Validation | Final Manuscript Outcome |
|---|---|---|---|
| **Descriptor interpretation (AATSC5i_A, AATS8v_A)** | Overconfident mechanistic narratives from correlation (e.g., "creates contiguous hydrophilic domains facilitating $OH^-$ transport") | Revised to hypothesis-level language; cross-checked against relevant AEM literature | Conservative phrasing: "consistent with," "may reflect," "suggests" |
| **Design threshold identification** | Screening-threshold heuristics (e.g., AATSC5i_A > 0, AATS8v_A > 140) implying monotonic improvement | Expert analysis of high-conductivity subset revealed non-monotonic tradeoffs | Refined to "optimal balance window" acknowledging upper limits |
| **Length-scale significance (lag-5, lag-8)** | Non-proactive: explanation provided only after explicit expert prompting | Domain knowledge required to formulate the appropriate question | Explicit connection to typical AEM side-chain architectures (7–8 σ-bonds) |
| **Structural design suggestions** | Generic suggestions without feasibility/stability context (e.g., "introduce heavier hetero-atoms") | Expert screening through established AEM synthesis knowledge | Retained only chemically plausible, synthetically accessible motifs |
| **Statistical claims** | Reports/derives statistics from supplied data without formal reproducibility context | Recomputed and confirmed in author scripts; only verified values reported | Statistics in manuscript derived from author-produced scripts |

**Table S10**. Predicted anion conductivity profiles for AEM Polymers 1 and 3 under varying conditions. Temperature-dependent conductivity is shown at 20, 40, 60, and 80 °C (0 days alkaline exposure), followed by time-resolved alkaline degradation predictions at 80 °C over 0–100 days of exposure (1 M NaOH, 60 °C). Single-point predictions at 80 °C (0 days) are included for AEM Polymers 2 and 4 for reference. All predictions were performed using Model II-mini with IEC values calculated from the designed structures.

| **AEM Polymer No.** | **AATSC5i_A** | **AATS8v_A** | **IEC** | **alkaline stability / Days** | **Conductivity Measuring Temperature / °C** | **Predicted anion conductivity / S cm$^{-1}$** |
|---|---|---|---|---|---|---|
| 1 | 0.07185 | 139.1117 | 2.40 | 0 | 20 | 0.04871 |
| 1 | 0.07185 | 139.1117 | 2.40 | 0 | 40 | 0.06682 |
| 1 | 0.07185 | 139.1117 | 2.40 | 0 | 60 | 0.08807 |
| 1 | 0.07185 | 139.1117 | 2.40 | 0 | 80 | 0.11244 |
| 1 | 0.07185 | 139.1117 | 2.40 | 1 | 80 | 0.11151 |
| 1 | 0.07185 | 139.1117 | 2.40 | 2 | 80 | 0.11059 |
| 1 | 0.07185 | 139.1117 | 2.40 | 3 | 80 | 0.10969 |
| 1 | 0.07185 | 139.1117 | 2.40 | 4 | 80 | 0.10881 |
| 1 | 0.07185 | 139.1117 | 2.40 | 5 | 80 | 0.10794 |
| 1 | 0.07185 | 139.1117 | 2.40 | 6 | 80 | 0.10709 |
| 1 | 0.07185 | 139.1117 | 2.40 | 7 | 80 | 0.10625 |
| 1 | 0.07185 | 139.1117 | 2.40 | 8 | 80 | 0.10543 |
| 1 | 0.07185 | 139.1117 | 2.40 | 9 | 80 | 0.10462 |
| 1 | 0.07185 | 139.1117 | 2.40 | 10 | 80 | 0.10383 |
| 1 | 0.07185 | 139.1117 | 2.40 | 100 | 80 | 0.07639 |
| 2 | −0.06804 | 127.0347 | 2.08 | 0 | 80 | 0.07410 |
| 3 | 0.09846 | 161.8823 | 1.70 | 0 | 20 | 0.05211 |
| 3 | 0.09846 | 161.8823 | 1.70 | 0 | 40 | 0.06690 |
| 3 | 0.09846 | 161.8823 | 1.70 | 0 | 60 | 0.08368 |
| 3 | 0.09846 | 161.8823 | 1.70 | 0 | 80 | 0.10242 |
| 3 | 0.09846 | 161.8823 | 1.70 | 1 | 80 | 0.10157 |
| 3 | 0.09846 | 161.8823 | 1.70 | 2 | 80 | 0.10072 |
| 3 | 0.09846 | 161.8823 | 1.70 | 3 | 80 | 0.09989 |
| 3 | 0.09846 | 161.8823 | 1.70 | 4 | 80 | 0.09907 |
| 3 | 0.09846 | 161.8823 | 1.70 | 5 | 80 | 0.09827 |
| 3 | 0.09846 | 161.8823 | 1.70 | 6 | 80 | 0.09747 |
| 3 | 0.09846 | 161.8823 | 1.70 | 7 | 80 | 0.09668 |
| 3 | 0.09846 | 161.8823 | 1.70 | 8 | 80 | 0.09591 |
| 3 | 0.09846 | 161.8823 | 1.70 | 9 | 80 | 0.09515 |
| 3 | 0.09846 | 161.8823 | 1.70 | 10 | 80 | 0.09440 |
| 3 | 0.09846 | 161.8823 | 1.70 | 100 | 80 | 0.07306 |
| 4 | 0.1087 | 162.3189 | 1.56 | 0 | 80 | 0.07265 |

**Table S11**. Representative snapshot of the AEM polymer database showing raw experimental parameters. The complete database contains 2,452 entries from 346 unique polymers and is openly available on GitHub (https://github.com/KatoGroup-AppChemKU/AEM_Unsupervised-ML).[4]

| Membrane Name (abbreviation) | Block A (x) | Block B (1-x) | Block A/B ratio | Polymer type | Conductivity Measuring Temperature [oC] | Membrane Anion Conductivity [S/cm] | ABC_A | |
|---|---|---|---|---|---|---|---|---|
| **PAEK-PYR50** | 0.198 | 0.802 | 0.247 | 1 | 80 | 0.00318 | 35.04061 | |
| **PAEK-PYR75** | 0.502 | 0.498 | 1.008 | 1 | 80 | 0.00616 | 35.04061 | … |
| **PAEK-PYR100** | 0.7581 | 0.2419 | 3.134 | 1 | 80 | 0.01026 | 35.04061 | |
| **PAEK-PYR125** | 0.967 | 0.033 | 29.303 | 1 | 80 | 0.01156 | 35.04061 | |
| | | | | ⋮ | | | | |

## Data / Code Availability

The source code and database used in this study are available in GitHub (github.com/KatoGroup-AppChem-KU/AEM_Explainable-ML_Workflow) to promote the introduction of machine learning within the community.

## References

(1) Ding, C.; Peng, H. Minimum Redundancy Feature Selection from Microarray Gene Expression Data. *J. Bioinform. Comput. Biol*. **2005**, 3 (2), 185-205. DOI: 10.1142/s0219720005001004.
(2) Radovic, M.; Ghalwash, M.; Filipovic, N.; Obradovic, Z. Minimum Redundancy Maximum Relevance Feature Selection Approach for Temporal Gene Expression Data. *BMC Bioinformatics* **2017**, 18 (1), 9. DOI: 10.1186/s12859-016-1423-9.
(3) Liu, D.; Lin, L.; Xie, Y.; Pang, J.; Jiang, Z. Anion exchange membrane based on poly(arylene ether ketone) containing long alkyl densely quaternized carbazole derivative pendant. *J. Membr. Sci.* **2021**, 623, 119079. DOI: 10.1016/j.memsci.2021.119079.
(4) Phua, Y. K.; Terasoba, N.; Tanaka, M.; Fujigaya, T.; Kato, K. Unsupervised Machine Learning-Derived Anion-Exchange Membrane Polymers Map: A Guideline for Polymers Exploration and Design. *ChemElectroChem* **2024**, 11 (14), e202400252. DOI: 10.1002/celc.202400252.